

6. Drift Chamber

6.1. Purpose and Design Requirements

The principal purpose of the drift chamber (DCH) is the efficient detection of charged particles and the measurement of their momenta and angles with high precision. These high precision measurements enable the reconstruction of exclusive B - and D -meson decays with minimal background. The DCH complements the measurements of the impact parameter and the directions of charged tracks provided by the SVT near the IP. At lower momenta, the DCH measurements dominate the errors on the extrapolation of charged tracks to the DIRC, EMC, and IFR.

The reconstruction of decay and interaction vertices outside of the SVT volume, for instance the K_s^0 decays, relies solely on the DCH. For this purpose, the chamber should be able to measure not only the transverse momenta and positions, but also the longitudinal position of tracks, with a resolution of ~ 1 mm.

The DCH also needs to supply information for the charged particle trigger with a maximum time jitter of $0.5 \mu\text{s}$ (Section 11).

For low momentum particles, the DCH is required to provide particle identification by measurement of ionization loss (dE/dx). A resolution of about 7% will allow π/K separation up to $700 \text{ MeV}/c$. This capability is complementary to that of the DIRC in the barrel region, while in the extreme backward and forward directions, the DCH is the only device providing some discrimination of particles of different mass.

Since the average momentum of charged particles produced in B - and D -meson decays is less than $1 \text{ GeV}/c$, multiple scattering is a significant, if not the dominant limitation on the track parameter resolution. In order to reduce this contribution, material in front of and inside the chamber volume has to be minimized.

Finally, the DCH must be operational in the presence of large beam-generated backgrounds, which were predicted to generate rates of $\sim 5 \text{ kHz}/\text{cell}$ in the innermost layers.

6.2. Mechanical Design and Assembly

6.2.1. Overview

The DCH is relatively small in diameter, but almost 3 m long, with 40 layers of small hexagonal cells providing up to 40 spatial and ionization loss measurements for charged particles with transverse momentum greater than $180 \text{ MeV}/c$. Longitudinal position information is obtained by placing the wires in 24 of the 40 layers at small angles with respect to the z -axis. By choosing low-mass aluminum field wires and a helium-based gas mixture, the multiple scattering inside the DCH is held to a minimum, less than $0.2\% X_0$ of material. The properties of the chosen gas, a 80:20 mixture of helium:isobutane, are presented in Table 8. This mixture has a radiation length that is five times larger than commonly used argon-based gases. The smaller Lorentz angle results in a rather uniform time-distance relationship and thereby improved spatial resolution.

Table 8

Properties of helium-isobutane gas mixture at atmospheric pressure and 20°C . The drift velocity is given for operation without magnetic field, while the Lorentz angle is stated for a 1.5 T magnetic field.

Parameter	Values
Mixture He : C ₄ H ₁₀	80:20
Radiation Length	807 m
Primary Ions	21.2/cm
Drift Velocity	22 $\mu\text{m}/\text{ns}$
Lorentz Angle	32°
dE/dx Resolution	6.9%

The inner cylindrical wall of the DCH is kept thin to facilitate the matching of the SVT and DCH tracks, to improve the track resolution for high momentum tracks, and to minimize the background from photon conversions and interactions. Material in the outer wall and in the forward direction is also minimized so as not to degrade the performance of the DIRC and the EMC. For this reason, the HV distribution and all of the readout electronics are mounted on the

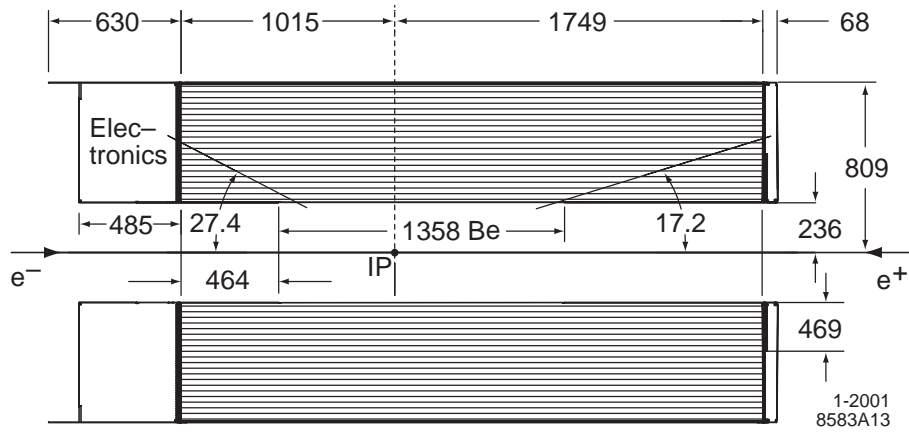


Figure 28. Longitudinal section of the DCH with principal dimensions; the chamber center is offset by 370 mm from the interaction point (IP).

backward endplate of the chamber. This choice also eliminates the need for a massive, heavily shielded cable plant.

A longitudinal cross section and dimensions of the DCH are shown in Figure 28. The DCH is bounded radially by the support tube at its inner radius and the DIRC at its outer radius. The device is asymmetrically located with respect to the IP. The forward length of 1749 mm is chosen so that particles emitted at polar angles of 17.2° traverse at least half of the layers of the chamber before exiting through the front endplate. In the backward direction, the length of 1015 mm means that particles with polar angles down to 152.6° traverse at least half of the layers. This choice ensures sufficient coverage for forward-going tracks, and thus avoids significant degradation of the invariant mass resolution, while at the same time maintaining a good safety margin on the electrical stability of the chamber. The DCH extends beyond the endplate by 485 mm at the backward end to accommodate the readout electronics, cables, and an rf shield. It extends beyond the forward endplate by 68 mm to provide space for wire feed-throughs and an rf shield.

6.2.2. Structural Components

Details of the DCH mechanical design are presented in Figure 29. The endplates, which carry an axial load of 31,800 kN, are made from alu-

minum plates of 24 mm thickness. At the forward end, this thickness is reduced to 12 mm beyond a radius of 46.9 cm to minimize the material in front of the calorimeter endcap. For this thickness, the estimated safety margin on the plastic yield point for endplate material (6061T651 aluminum) is not more than a factor of two. The maximum total deflection of the endplates under loading is small, about 2 mm or 28% of the 7 mm wire elongation under tension. During installation of the wires, this small deflection was taken into account by over-tensioning the wires.

The inner and outer cylinder cylindrical walls are load bearing to reduce the maximum stress and deflections of the endplates. The stepped forward endplate created a complication during the assembly, because the thinner forward endplate would deflect more than the thicker backward endplate. The outside rim of the forward endplate had to be pre-loaded, *i.e.*, displaced by 2.17 mm in the forward direction, to maintain the inside and outside rims of the rear endplate at the same longitudinal position after the load of the wires was transferred from the stringing fixture to the outer cylinder.

Prior to installation on the inner cylinder, the two endplates were inspected on a coordinate-measuring machine. All sense wire holes, as well as 5% of the field and clearing field wire holes, were measured to determine their absolute loca-

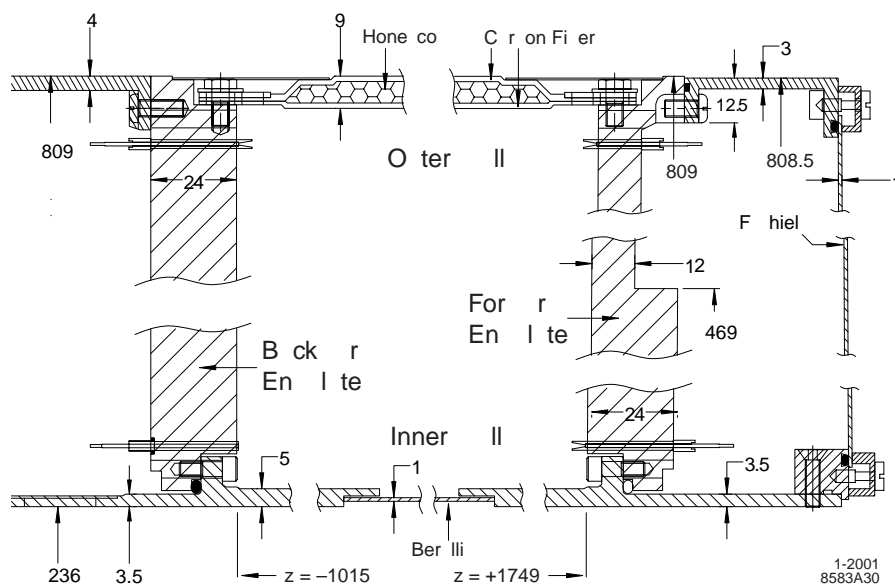


Figure 29. Details of the structural elements of the DCH. All components are made of aluminum, except for the 1 mm-thick inner beryllium wall and the 9 mm-thick outer composite wall.

tions. The achieved accuracy of the hole placement was $38\ \mu\text{m}$ for both sense and field wires, better than the specification by more than a factor of two. In addition, the diameters of the same sample of endplate holes were checked with precision gauge pins. All holes passed the diameter specification (4.500 ± 0.025 for sense wires and 2.500 ± 0.025 for the field and guard wires).

The inner cylindrical wall of the DCH, which carries 40% of the wire load, was made from five sections, a central 1 mm-thick beryllium tube with two aluminum extensions which were in turn electron-beam welded to two aluminum end flanges to form a 3 m-long cylindrical part. The central section was made from three 120° segments of rolled and brazed beryllium. The end flanges have precision surfaces onto which the endplates were mounted. These surfaces set the angles of the two endplates with respect to the axis and significantly constrain the concentricity of the tube. The inner cylinder also provides a substantial rf shield down to the PEP-II bunch-gap frequency of 136 kHz.

The outer wall bears 60% of axial wire load between the endplates. To simplify its installa-

tion, this external wall was constructed from two half-cylinders with longitudinal and circumferential joints. The gas and electrical seals for these joints were made up *in situ*. The main structural element consists of two 1.6 mm-thick ($0.006X_0$) carbon fiber skins laminated to a 6 mm-thick honeycomb core. The outer shell is capable of withstanding a differential pressure of 30 mbar and temperature variations as large as $\pm 20^\circ\text{C}$, conditions that could be encountered during shipping or installation. Aluminum foil, $25\ \mu\text{m}$ -thick on the inside surface and $100\ \mu\text{m}$ on the outside, are in good electrical contact with the endplates, thereby completing the rf shield for the chamber.

The total thickness of the DCH at normal incidence is $1.08\%X_0$, of which the wires and gas mixture contribute $0.2\%X_0$, and the inner wall $0.28\%X_0$.

6.2.3. Wire Feed-Throughs

A total of five different types of feed-throughs were required for the chamber to accommodate the sense, field, and clearing field wires, as well as two different endplate thicknesses. The five types are illustrated in Figure 30. They incorporate crimp pins [43] of a simple design which fasten

and precisely locate the wires. The choice of pin material (gold-plated copper for the signal wires and gold-plated aluminum for the field wires) and wall thickness in the crimp region was optimized to provide an allowable range of almost $150\ \mu\text{m}$ in crimp size, as a primary means for avoiding wire breakage.

Crimp pins were either press-fit into an insulator made from a single piece of injection-molded thermoplastic reinforced with 30% silica glass fiber [44], or swaged into a copper jacket for the field wires. The plastic insulates the sense, guard, and clearing field wires from the electrically grounded endplates, while the metal jackets provide good ground contact for field wires ($< 0.1\ \Omega$) on the backward endplate. The outer diameter of the field and clearing field feed-throughs was maintained at $2.000^{+0.000}_{-0.025}$ mm while the sense wire feed-through had a larger ($4.500^{+0.000}_{-0.025}$ mm) outer diameter and a longer body (41.7 mm). This choice provided both thicker insulating walls and a longer projection into the gas volume to better shield the HV from the grounded endplate.

6.2.4. Assembly and Stringing

Assembly of the chamber components and installation of the wires was carried out in a large clean room (Class 10,000) at TRIUMF in Vancouver. The wires were strung horizontally without the outer cylindrical shell in place. The endplates were mounted and aligned onto the inner cylinder which in turn was supported by a central shaft in a mobile fixture. The endplates were mounted on the inner cylinder at the inside rim and attached to support rings at the outside. These rings were connected by radial *spiders* to the central shaft of the stringing frame.

Two teams of two operators each worked in parallel as the wires were strung from the inner radius outward. The two teams were each assisted by an automated wire transporter [45]. A wire was attached to a needle which was inserted through one of the endplate hole, captured magnetically by one of the transporters, and then transported and inserted through the appropriate hole in the other endplate. The wire was then threaded through the feed-throughs, which were glued into the endplates, and the wire was ten-

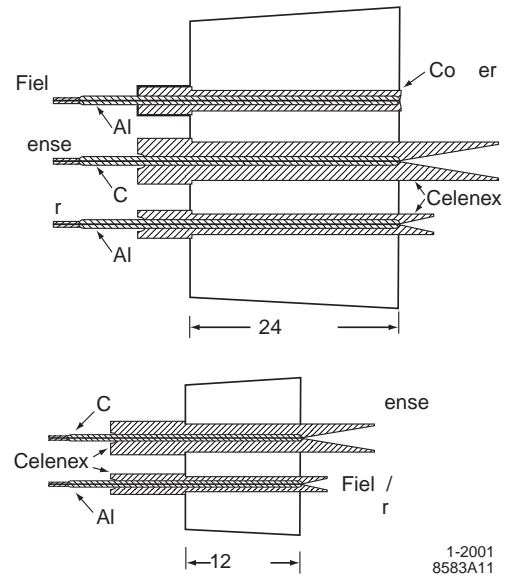


Figure 30. Design of the five DCH wire feed-throughs for the 24 mm-thick endplates and the 12 mm-thick endplate. The copper jacketed feed-through is for grounded field wires, the other four are for grounded sense wires (4.5 mm diameter), and guard and clearing field wires (2.5 mm diameter), all made from a Celenex insulator surrounding the crimp pins.

sioned and crimped. The automated wire transporters were largely built from industrial components, employing commercial software and hardware. The semi-automatic stringing procedure ensured the correct hole selection, accelerated the stringing rate and greatly improved the cleanliness and quality of the stringing process. The installation of a total of 28,768 wires was completed in less than 15 weeks.

6.3. Drift Cells

6.3.1. Layer Arrangement

The DCH consists of a total of 7,104 small drift cells, arranged in 40 cylindrical layers. The layers are grouped by four into ten superlayers, with the same wire orientation and equal numbers of cells in each layer of a superlayer. Sequential layers are staggered by half a cell. This arrangement enables local segment finding and left-right ambiguity resolution within a superlayer, even if one

out of four signals is missing. The stereo angles of the superlayers alternate between axial (A) and stereo (U,V) pairs, in the order AUVAUVAUVA, as shown in Figure 31. The stereo angles vary between ± 45 mrad and ± 76 mrad; they have been chosen such that the drilling patterns are identical for the two endplates. The hole pattern has a 16-fold azimuthal symmetry which is well suited to the modularity of the electronic readout and trigger system. Table 9 summarizes parameters for all superlayers.

Table 9

The DCH superlayer (SL) structure, specifying the number of cells per layer, radius of the innermost sense wire layer, the cell widths, and wire stereo angles, which vary over the four layers in a superlayer as indicated. The radii and widths are specified at the mid-length of the chamber.

SL	# of Cells	Radius (mm)	Width (mm)	Angle (mrad)
1	96	260.4	17.0-19.4	0
2	112	312.4	17.5-19.5	45-50
3	128	363.4	17.8-19.6	-(52-57)
4	144	422.7	18.4-20.0	0
5	176	476.6	16.9-18.2	56-60
6	192	526.1	17.2-18.3	-(63-57)
7	208	585.4	17.7-18.8	0
8	224	636.7	17.8-18.8	65-69
9	240	688.0	18.0-18.9	-(72-76)
10	256	747.2	18.3-19.2	0

6.3.2. Cell Design and Wires

The drift cells are hexagonal in shape, 11.9 mm by approximately 19.0 mm along the radial and azimuthal directions, respectively. The hexagonal cell configuration is desirable because approximate circular symmetry can be achieved over a large portion of the cell. The choice of aspect ratio has the benefit of decreasing the number of wires and electronic channels, while allowing a 40-layer chamber in a confined radial space. Each cell consists of one sense wire surrounded by six field wires, as shown in Figure 31. The properties of the different types of gold-coated wires that

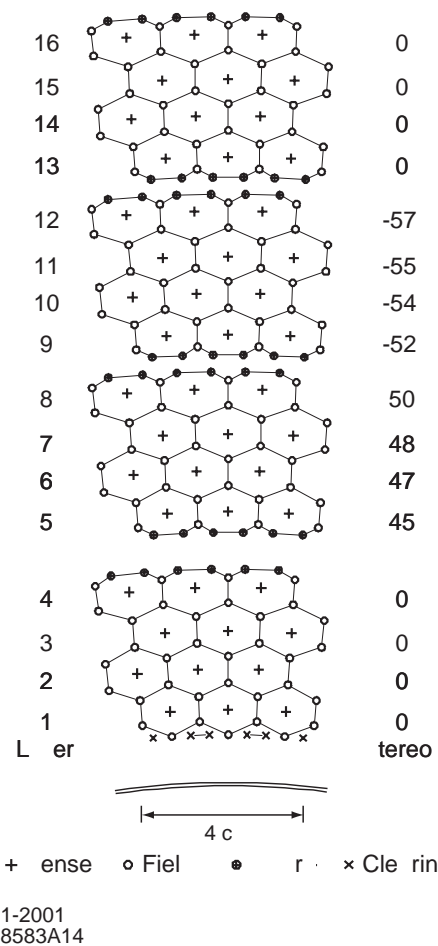


Figure 31. Schematic layout of drift cells for the four innermost superlayers. Lines have been added between field wires to aid in visualization of the cell boundaries. The numbers on the right side give the stereo angles (mrad) of sense wires in each layer. The 1 mm-thick beryllium inner wall is shown inside of the first layer.

make up the drift cells are given in Table 10. The sense wires are made of tungsten-rhenium [46], 20 μ m in diameter and tensioned with a weight of 30 g. The deflection due to gravity is 200 μ m at mid-length. Tungsten-rhenium has a substantially higher linear resistivity (290 Ω /m), compared to pure tungsten (160 Ω /m), but it is considerably stronger and has better surface quality. While the field wires are at ground potential, a

positive high voltage is applied to the sense wires. An avalanche gain of approximately 5×10^4 is obtained at a typical operating voltage of 1960 V and a 80:20 helium:isobutane gas mixture.

Table 10
DCH wire specifications (all wires are gold plated).

Type	Material	Diameter (μm)	Voltage (V)	Tension (g)
Sense	W-Re	20	1960	30
Field	Al	120	0	155
Guard	Al	80	340	74
Clearing	Al	120	825	155

The relatively low tension on the approximately 2.75 m-long sense wires was chosen so that the aluminum field wires have matching gravitational sag and are tensioned well below the elastic limit. A simulation of the electrostatic forces shows that the cell configuration has no instability problems. At the nominal operating voltage of 1960 V, the wires deflect by less than $60 \mu\text{m}$.

The field wires [47] are tensioned with 155 g to match the gravitational sag of the sense wires to within $20 \mu\text{m}$. This tension is less than one-half the tensile yield strength of the aluminum wire. For cells at the inner or outer boundary of a superlayer, two guard wires are added to improve the electrostatic performance of the cell and to match the gain of the boundary cells to those of the cells in the inner layers. At the innermost boundary of layer 1 and the outermost boundary of layer 40, two clearing wires have been added per cell to collect charges created through photon conversions in the material of the walls.

6.3.3. Drift Isochrones

The calculated isochrones and drift paths for ions in adjacent cells of layer 3 and 4 of an axial superlayer are presented in Figure 32. The isochrones are circular near the sense wires, but deviate greatly from circles near the field wires. Ions originating in the gap between superlayers are collected by cells in the edge layers after a delay of several μs . These lagging ions do not affect

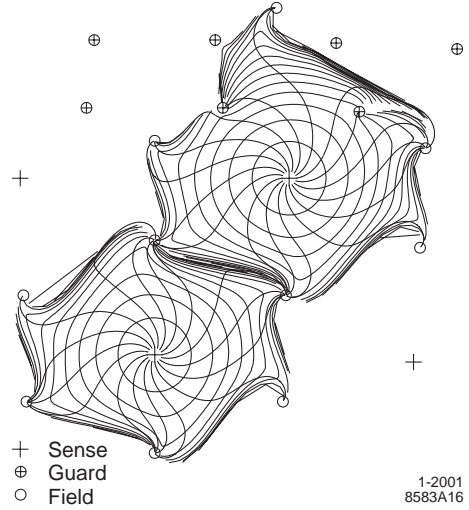


Figure 32. Drift cell isochrones, *i.e.*, contours of equal drift times of ions in cells of layers 3 and 4 of an axial superlayer. The isochrones are spaced by 100 ns. They are circular near the sense wires, but become irregular near the field wires, and extend into the gap between superlayers.

the drift times measurements, but they contribute to the dE/dx measurement.

6.3.4. Cross Talk

A signal on one sense wire produces oppositely-charged signals on neighboring wires due to capacitive coupling. The cross talk is largest between adjacent cells of adjacent layers, ranging from -0.5% at a superlayer boundary to -2.7% for internal layers within superlayers. For adjacent cells in the same layer, the cross talk ranges from -0.8 to -1.8% , while for cells separated by two layers it is less than 0.5% .

6.4. Electronics

6.4.1. Design Requirements and Overview

The DCH electronic system is designed to provide a measurement of the drift time and the integrated charge, as well as a single bit to the trigger system [48] for every wire with a signal. In the 80:20 helium:isobutane gas mixture, there are on average some 22 primary and 44 total ionization clusters produced per cm. The position of the primary ionization clusters is derived from timing of the leading edge of the amplified signal.

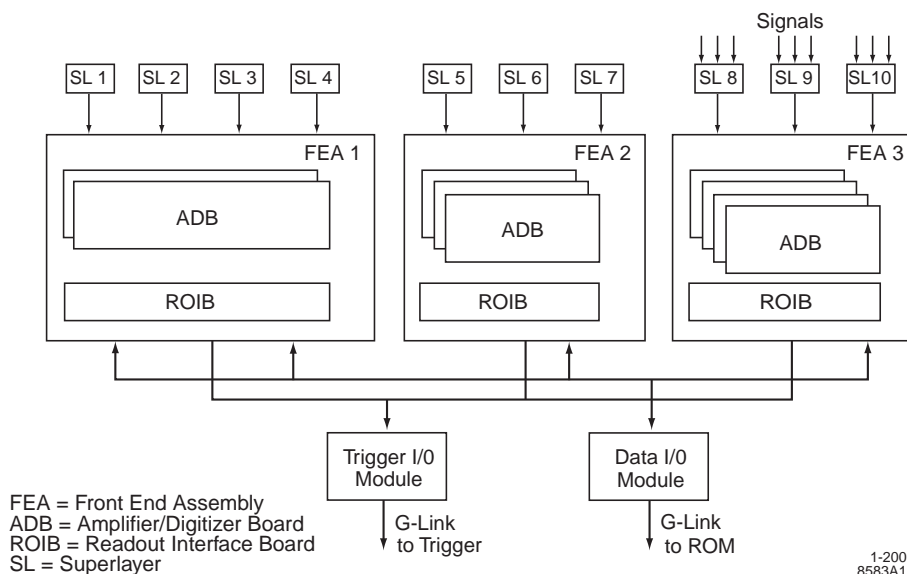


Figure 33. Block diagram for a $1/16^{\text{th}}$ wedge of the DCH readout system, showing logical organization of the three front-end assemblies and their connections to the trigger and data I/O modules

The design goal was to achieve a position resolution of $140\ \mu\text{m}$, averaged over the cells. To reduce the time jitter in the signal arrival and at the same time maintain a good signal-to-noise ratio, the signal threshold was set at about 2.5 primary electrons. For the dE/dx measurement, a resolution of 7% was projected for a 40-layer chamber.

The small cell size and the difficult access through the DIRC strong support tube require a very high density of electronics components. As a consequence, a compact and highly modular design was chosen. The readout is installed in well shielded assemblies that are plugged into the endplate and are easily removable for maintenance.

A schematic overview of the DCH electronics is presented in Figure 33 [49]. The 16-fold azimuthal symmetry of the cell pattern is reflected in the readout segmentation. The DCH amplifier and digitizer electronics are installed in electronics front-end assemblies (FEAs) that are mounted directly onto the rear endplate. There are three FEAs in each of the 16 sectors. These sectors are separated by brass cooling bars that extend from the inner to the outer chamber walls. These

bars provide mechanical support and water cooling channel for the FEAs. The assemblies connect to the sense wires through service boards, which route the signals and HV distribution. A readout interface board (ROIB) in each FEA organizes the readout of the digitized data. Data I/O and trigger I/O modules multiplex serial data from the FEAs to high-speed optical fibers for transfer to the readout modules that are located in the electronics building.

6.4.2. Service Boards

Service boards provide the electrostatic potentials for signal, guard, and clearing wires, and pass signals and ground to the front-end readout electronics. A side view of a service board is shown in Figure 34. The HV board contains the HV buses and filtering, current limiting resistors, and blocking capacitors. Jumpers connect adjacent boards. The stored energy is minimized by using a 220 pF HV blocking capacitors.

The signals are connected via series resistors to the upper signal board which contains the protection diodes and standard output connectors. Mounting posts, anchored into the rear endplate, also serve as ground connections.

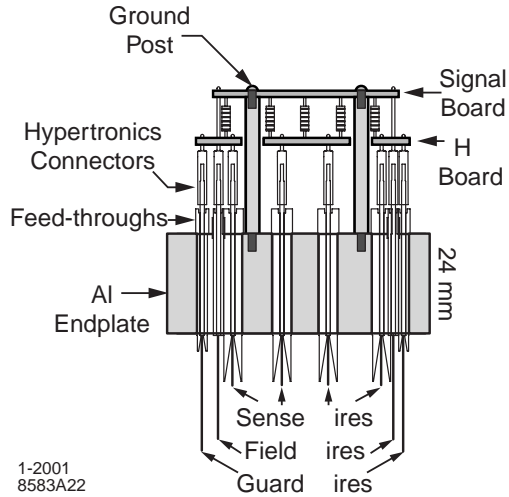


Figure 34. Side view of service boards showing two-tiered structure for DCH HV distribution and signal collection.

6.4.3. Front-End Assemblies

The FEAs plug into connectors on the back side of the service boards. These custom wedge-shaped crates are aluminum boxes that contain a ROIB and two, three, or four amplifier/digitizer boards (ADB) for superlayers 1–4, 5–7, and 8–10, respectively, as shown in Figure 35. The crates are mounted with good thermal contact to the water cooled radial support bars. The total heat load generated by the FEAs is 1.3 kW.

The ADBs are built from basic building blocks consisting of two 4-channel amplifier ICs [50] feeding a single 8-channel digitizer custom ASIC [51]. The number of channels serviced by an ADB is 60, 48, or 45, for the inner, middle, and outer FEA modules, respectively.

The custom amplifier IC receives the input signal from the sense wire and produces a discriminator output signal for the drift time measurement and a shaped analog signal for the dE/dx measurement. Both outputs are fully differential. The discriminator has gain and bandwidth control, and a voltage controlled threshold. The analog circuit has integrator and gain control.

The custom digitizer IC incorporates a 4-bit TDC for time measurement and a 6-bit 15 MHz FADC to measure the total deposited charge.

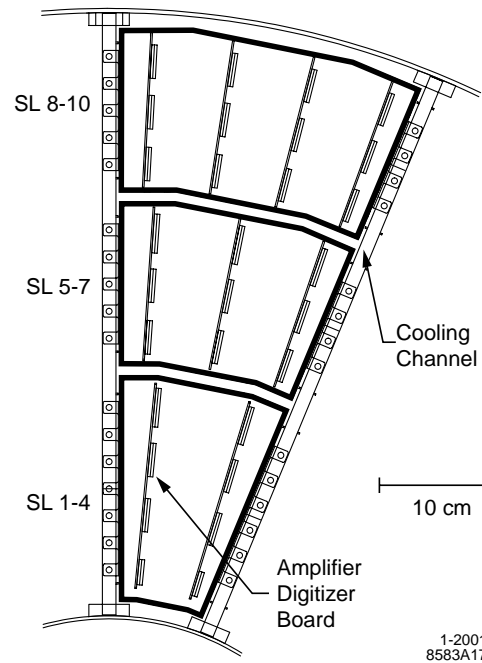


Figure 35. Layout of $1/16^{th}$ of the DCH rear endplate, showing three FEA boxes between water cooled channels.

The TDC is a phase-locked digital delay linear vernier on the sample clock of 15 MHz, which achieves a 1 ns precision for leading edge timing. The FADC design is based on a resistor-divider comparator ladder that operates in bilinear mode to cover the full dynamic range. The digitized output signals are stored in a trigger latency buffer for $12.9 \mu\text{s}$, after which a L1 *Accept* initiates the transfer of a $2.2 \mu\text{s}$ block of data to the readout buffer. In addition, trigger information is supplied for every channel, based either on the presence of a TDC hit during the sample period or FADC differential pulse height information, should a higher discriminator level be desirable.

The ROIB interprets FCTS commands to control the flow of data and trigger information. Data are moved to FIFOs on the ROIBs, and then to data and trigger I/O modules via 59.5 MHz serial links. A total of four such links are required per $1/16^{th}$ wedge, one for each of the outer two FEAs and two for the innermost of the FEA. Each

data I/O module services all FEAs one quadrant and transmits the data to a single ROM via one optical fiber link. The trigger stream is first multiplexed onto a total of 30 serial lines per wedge for transmission to the trigger I/O module. Trigger data from two wedges of FEAs are then transmitted to the trigger system via three optical links. Thus, a total of 28 optical fibers, four for the data and 24 for the charged particle trigger, are required to transfer the DCH data to the readout.

6.4.4. Data Acquisition

The data stream is received and controlled by four *BABAR* standard readout modules. Drift chamber-specific feature extraction algorithms convert the raw FADC and TDC information into drift times, total charge, and a status word. The time and charge are corrected channel-by-channel for time offsets, pedestals, and gain constants. Based on measurements of the noise a threshold is typically 2–3 electrons is applied to discriminate signals. These algorithms take about $1\ \mu\text{s}$ per channel, and reduce the data volume by roughly a factor of four.

6.4.5. High Voltage System

The HV bias lines on the chamber are daisy-chained together so that each superlayer requires only four power supplies, except for superlayer 1 which has eight. The voltages are supplied to the sense, guard, and clearing wires by a CAEN SY527 HV mainframe [42], equipped with 24-channel plug-in modules. The sense wires are supplied by 44 HV channels providing up to $40\ \mu\text{A}$ of current each that can be monitored with a resolution of 0.1%.

6.5. Gas System

The gas system has been designed to provide a stable 80:20 helium:isobutane mixture at a constant over pressure of 4 mbar [52]. The chamber volume is about $5.2\ \text{m}^3$. Gas mixing and recirculation is controlled by precise mass flow controllers; the total flow is tuned to $15\ \ell/\text{min}$, of which $2.5\ \ell/\text{min}$ are fresh gas. During normal operation, the complete DCH gas volume is recirculated in six hours, and one full volume of fresh gas is added every 36 hours. The pressure

in the DCH is measured by two independent pressure gauges, one of which is connected to a regulator controlling the speed of the compressor. The relative pressure in the chamber is controlled to better than ± 0.05 mbar.

Oxygen is removed from the gas mixture using a palladium catalytic filter. The water content is maintained at 3500 ± 200 ppm by passing an adjustable fraction of the gas through a water bubbler. This relatively high level of water vapor is maintained to prevent electrical discharge. In addition to various sensors to monitor pressure, temperature, and flow at several points of the system, a small wire chamber with an ^{55}Fe source continuously monitors gain of the gas mixture.

6.6. Calibrations and Monitoring

6.7. Electronics Calibration

The front-end electronics (FEEs) are calibrated daily to determine the channel-by-channel correction constants and thresholds. Calibration pulses are produced internally and input to the preamplifier at a rate of about 160 Hz. The calibration signals are processed in the ROM to minimize the data transfer and fully exploit the available processing power. The results are stored for subsequent feature extraction. The entire online calibration procedure takes less than two minutes.

6.7.1. Environmental Monitoring

The operating conditions of the DCH are monitored in realtime by a variety of sensors and read out by the detector-wide CAN bus system. These sensors monitor the flow rate, pressure, and gas mixture; the voltages and currents applied to the wires in the chamber; the voltages and currents distributed to the electronics from power supplies and regulators; instantaneous and cumulative radiation doses; temperature and humidity around the chamber electronics and in the equipment racks. Additional sensors monitor the atmosphere in and around the detector for excess isobutane, which could pose a flammability or explosive hazard in the event of a leak.

Many of the sensors are connected to hardware interlocks, which ensure that the chamber is automatically put into a safe state in response to an unsafe condition. All of these systems have per-

formed reliably. In addition, automated software monitors raw data quality, chamber occupancies and efficiencies to sense variations in electronics performance that might indicate more subtle operational problems.

6.7.2. Operational Experience

The design of the DCH specifies a voltage of 1960 V on the sense wires to achieve the desired gain and resolution. The chamber voltage was lowered for part of the run to 1900 V out of concern for a small region of the chamber that was damaged during the commissioning phase by inadvertently applying 2 kV to the guard wires. Wires in this region (10.4% of superlayer 5, and 4.2% of superlayer 6) were disconnected when continuous discharge was observed over extended periods of time.

6.8. Performance

The DCH was first operated with full magnetic field immediately after the installation into *BABAR*. Cosmic ray data were recorded and extensive studies of the basic cell performance were performed to develop calibration algorithms for the time-to-distance and dE/dx measurements. These algorithms were then implemented as described below for colliding beam data. Calibrations are monitored continuously to provide feedback to the operation; some time varying parameters are updated continuously as part of OPR. For charge particle tracking the DCH and SVT information is combined; the performance of the combined tracking system is described in Section 7.

6.8.1. Time-to-Distance Relation

The precise relation between the measured drift time and drift distance is determined from samples of e^+e^- and $\mu^+\mu^-$ events. For each signal, the drift distance is estimated by computing the distance of closest approach between the track and the wire. To avoid bias, the fit does not use the hit on the wire under consideration. The estimated drift distances and measured drift times are averaged over all wires in a layer, but the data are accumulated separately for tracks passing on the left of a sense wire and on the right. The time-distance relation is fit to a sixth-order Chebychev polynomial. An example of such a fit is shown in

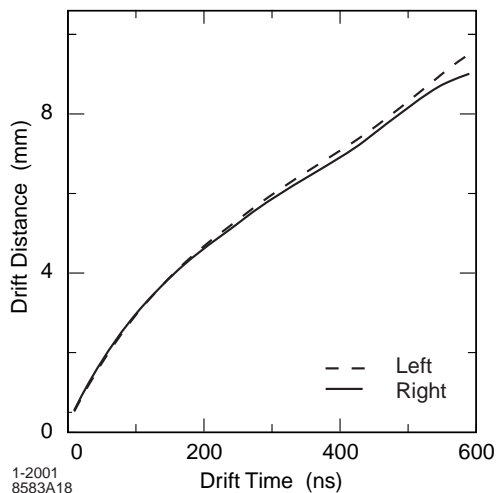


Figure 36. The drift time versus distance relation for left and right half of a cell. These functions are obtained from the data averaged over all cells in a single layer of the DCH.

Figure 36.

An additional correction is made for tracks with varying entrance angle into the drift cell. This angle is defined relative to the radial vector from the IP to the sense wire. The correction is applied as a scale factor to the drift distance and was determined layer-by-layer from a Garfield [53] simulation. The entrance angle correction is implemented as a tenth-order Chebychev polynomial of the drift distance, with coefficients which are functions of the entrance angle.

Figure 37 shows the position resolution as a function of the drift distance, separately for the left and the right side of the sense wire. The resolution is taken from Gaussian fits to the distributions of residuals obtained from unbiased track fits. The results are based on multi-hadron events, for data averaged over all cells in layer 18.

6.8.2. Charge Measurement

The specific energy loss, dE/dx , for charged particles traversing the DCH is derived from measurement of total charge deposited in each drift cell. The charge collected per signal cell is measured as part of the feature extraction algorithm in the ROM. Individual measurements are corrected for gain variations, pedestal-subtracted

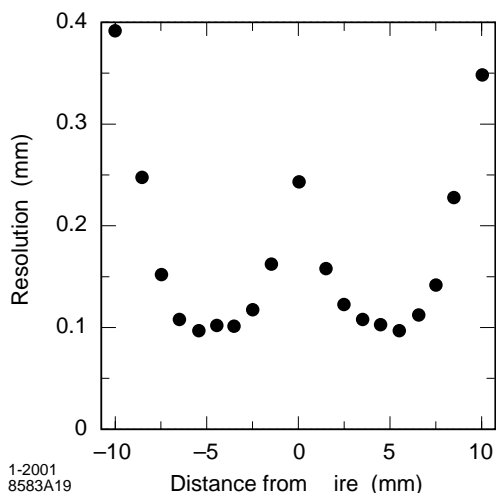


Figure 37. DCH position resolution as a function of the drift distance in layer 18, for tracks on the left and right side of the sense wire. The data are averaged over all cells in the layer.

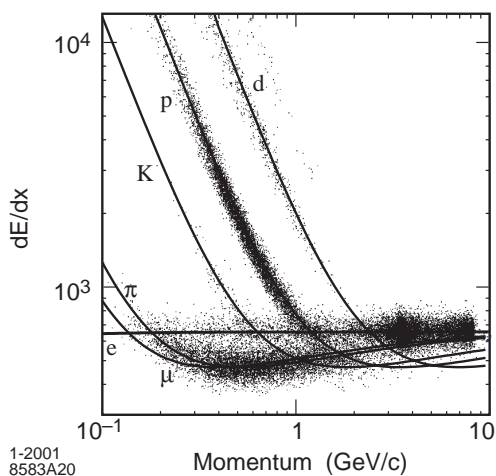


Figure 38. Measurement of dE/dx in the DCH as a function of track momenta. The data include large samples of beam background triggers, as evident from the high rate of protons. The curves show the Bethe-Bloch predictions derived from selected control samples of particles of different masses.

and integrated over a period of approximately $1.8 \mu\text{s}$.

The specific energy loss per track is computed as a truncated mean from the lowest 80% of the individual dE/dx measurements. Various corrections are applied to remove sources of bias that degrade the accuracy of the primary ionization measurement. These corrections include the following:

- changes in gas pressure and temperature, leading to $\pm 9\%$ variation in dE/dx , corrected by a single overall multiplicative constant;
- differences in cell geometry and charge collection ($\pm 8\%$ variation), corrected by a set of multiplicative constants for each wire;
- signal saturation due to space charge build-up ($\pm 11\%$ variation), corrected by a second-order polynomial in the dip angle, λ , of the form $1/\sqrt{\sin^2 \lambda + \text{const}}$;
- non-linearities in the most probable energy loss at large dip angles ($\pm 2.5\%$ variation), corrected with a fourth-order Chebychev polynomial as a function of λ ; and
- variation of cell charge collection as a function entrance angle ($\pm 2.5\%$ variation), corrected using a sixth-order Chebychev polynomial in the entrance angle.

The overall gas gain is updated continuously based on calibrations derived as part of prompt reconstruction of the colliding beam data; the remaining corrections are determined once for a given HV voltage setting and gas mixture.

Corrections applied at the single-cell level can be large compared to the single-cell dE/dx resolution, but have only a modest impact on the average resolution of the ensemble of hits. Global corrections applied to all hits on a track are therefore the most important for the resolution.

Figure 38 shows the distribution of the corrected dE/dx measurements as a function of track momenta. The superimposed Bethe-Bloch predictions for particles of different masses have been determined from selected control samples.

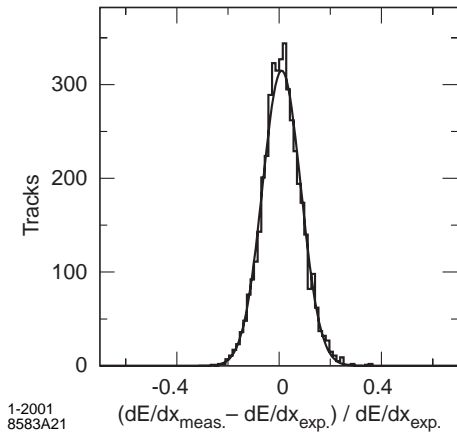


Figure 39. Difference between the measured and expected energy loss dE/dx for e^\pm from Bhabha scattering, measured in the DCH at an operating voltage of 1900 V. The curve represents a Gaussian fit to the data with a resolution of 7.5%.

The measured dE/dx resolution for Bhabha events is shown in Figure 39. The rms resolution achieved to date is typically 7.5%, limited by the number of samples and Landau fluctuations. This value is close to the expected resolution of 7%. Further refinements and additional corrections are being considered to improve performance.

6.9. Conclusions

The DCH has been performing close to design expectations from the start of operations. With the exception of a small number of wires that were damaged by an unfortunate HV incident during the commissioning phase, all cells are fully operational. The DCH performance has proven very stable over time. The design goal for the intrinsic position and dE/dx resolution have been met. Backgrounds are acceptable at present beam currents, but there is concern for rising occupancies and data acquisition capacity at the high end of the planned luminosity upgrades.